Hatzor, Y. H. & Goodman, R. E. (1997). *Géotechnique* **47**, No. 4, 817–839

Three-dimensional back-analysis of saturated rock slopes in discontinuous rock—a case study

Y. H. HATZOR* and R. E. GOODMAN†

Two historic block failures on the left abutment of Pacoima Dam, California, are back-analysed using three-dimensional limit equilibrium analysis. Water pressures within the boundary joints are introduced by parametric addition of vectors using enhanced stereographic projection. The magnitude and orientation of the resultant necessary to cause failure are established, as a function of the available friction angle. The influence of joint friction on the joint water pressure required to initiate block sliding and on the failure mode is discussed. It is shown that with increasing joint water pressure the orientation of the resultant dictates a changing failure *mode*, in the cases studied, from double plane to single plane sliding. The actual failure mode depends on the available friction angle of the joints. The influence of increasing joint water pressure on the factor of safety is also discussed. It is shown that the rotation of the resultant force by the addition of joint water forces rapidly reduces the factor of safety. The rate of change of the factor of safety with respect to joint water pressure in the base joints is shown to be higher for double plane sliding and lower for single plane sliding for the same block, when both failure modes are investigated. Block theory analysis is used to assess the stability of the right abutment of Pacoima Dam, presently concealed by a thick layer of gunite, and the critical blocks in the abutment are found using the procedure of Hatzor. It is demonstrated that in contrast to the unstable left abutment, the right abutment is perfectly safe, by virtue of kinematics alone. This theoretical result is strongly validated by the field performance of the right abutment, which experienced several episodes of strong ground motions in the past.

KEYWORDS: case history; dams; design; limit state design/analysis; slopes.

L'article présente une rétro-analyse de deux ruptures de bloc de la culée gauche du barrage de Pacoima en Californie. Cette analyse repose sur un examen de l'équilibre limite à trois dimensions. Les pressions de l'eau dans les joints limites sont introduites par l'addition paramétrique de vecteurs à l'aide d'une projection stéréographique améliorée. La grandeur et l'orientation de la résultante nécessaire à la rupture sont établies en fonction de l'angle de frottement disponible. Les auteurs examinent l'influence du frottement des joints sur la pression d'eau nécessaire à déclencher le glissement des blocs, ainsi que sur le mode de rupture. Ils montrent que, dans les cas étudiés, quand la pression de l'eau sur les joints augmente, l'orientation de la résultante dicte un changement du *mode* de rupture: un glissement dans un plan se substitue au glissement dans deux plans. Le mode de rupture dépend en fait de l'angle de frottement des joints. Les auteurs examinent aussi la façon dont l'augmentation de la pression de l'eau sur les joints modifie le coefficient de sécurité. Ils montrent que ce coefficient baisse rapidement sous l'effet de la rotation de la résultante provoquée par l'augmentation de la pression sur les joints. Quand ils ont examiné les deux modes de rupture, soit le glissement dans deux plans et le glissement dans un plan provoqués par la pression de l'eau sur les joints de base, ils ont constaté que, pour un même bloc, le coefficient de sécurité changeait plus rapidement dans un glissement dans deux plans que dans un glissement dans un plan. Les auteurs ont recours à l'analyse de la théorie des blocs pour évaluer le stabilité de la culée droite du barrage de Pacoima, actuellement dissimulée sous une épaisse couche de gunite, et à la méthode de Hatzor pour identifier les blocs *critiques* dans la culée. Ils démontrent que, contrairement à la culée gauche, qui est instable, la culée droite, rien que du fait de la cinématique, ne présente aucun danger. Ce résultat théorique est fortement validé par le comportement de la culée droite, qui, par le passé, a subi plusieurs grands mouvements de sol.

INTRODUCTION

Rock slope stability analysis must address rock discontinuities. In a pervasively fractured hard rock, conventional soil mechanics solutions are not relevant. Engineers have devised three different approaches to evaluate the stability of jointed rock slopes

(*a*) adaptation of soil mechanics solutions using the theory of elasticity and statics (e.g. Terzaghi, 1962; Bray, 1966, 1967; Jaeger, 1971; Hoek & Bray, 1981;
(*b*) limit equilibrium analysis formulated in three dimensions using vector methods (e.g. Hoek & Bray, 1981; Londe *et al.*, 1969; Bray & Brown, 1976)
(*c*) limit equilibrium and kinematic methods using stereographic projection and vector analysis (e.g. Hoek & Bray, 1981; Londe *et al.*, 1969, 1970; John, 1968; Goodman, 1976; Goodman & Shi, 1985).

Each of the three methods above has been used quite extensively by rock engineers over the past three decades. The first approach has been typically limited to a two-dimensional treament of simple joint patterns. Terzaghi (1962), for example, used soil mechanics techniques to analyse the stability of jointed rock slopes containing one potential surface of sliding; he strongly emphasized the adverse effect of joint water pressures on the stability of jointed rock slopes. Bray (1966, 1967) extended typical soil mechanics solutions and elasticity concepts to fractured and jointed rocks; he derived limit equilibrium equations suitable for some simple cases of joint patterns under a two-dimensional state of stress, but ignored the effect of joint water pressure. Jaeger (1971) pointed out that the fundamental difficulty in rock slope analysis is uncertainty in the law of friction for low values of normal stress. He used an elementary two-dimensional theory of stability of rock slopes for single and double plane sliding to show how the assumed friction law affects the factor of safety.

Solution methods based on vector analysis have been typically limited to the case of a tetrahedral wedge. The solutions (e.g. Bray & Brown, 1976) are nevertheless useful because they address the cases of single and double plane sliding, the only two possible modes of sliding failure, and they allow for water pressures inside the discontinuities.

Incorporation of stereographic projection techniques provides a fully three-dimensional graphical presentation of the problem and helps one visualize complex three-dimensional entities. It is necessary to emphasize, however, that all constructions on the stereographic projection can be performed by simple methods of vector analysis. Various workers (Hoek & Bray, 1981; Londe *et al.*, 1969, 1970; John, 1968; Goodman, 1976) have shown how vector analysis operations can be performed using the stereographic projection, and thus how limit equilibrium analysis can be achieved. Practical advance was introduced with block theory (Goodman & Shi, 1985). Founded on a rigorous mathematical base and incorporating concepts from topology and set theory, block theory provides kinematical tests for the removability of a block bounded by an arbitrary number of surfaces, in addition to finding the applicable failure mode and the state of static equilibrium. Using relatively simple block theory analyses, one can now achieve a comprehensive stability evaluation of jointed rock slopes, provided the geometry of the problem is clearly defined, and all active forces are known.

All methods discussed above assume a defined and predetermined rock mass geometry. Often in practice the engineer must extrapolate from an available set of data to a slope where the structure may not be exposed. This is especially crucial when a re-evaluation of a rock slope stability is necessary after the rock face has been concealed by a layer of shotcrete, for example in analysing the impact of a probable maximum flood (PMF) on the stability of existing dam abutments. This paper discusses the incorporation of statistical methods in block theory analysis in order to obtain critical key blocks, following the work by Hatzor (1993). In order to evaluate the sensitivity of critical block stability to water pressures, two historic block failures in the left abutment and the spillway of the Pacoima concrete gravity dam are back-analysed to establish the required water pressure to induce failure. The failures occurred during an intense rainstorm in 1938. The structural integrity of the right abutment, which remained intact during the same rainstorm and during the 6·6 magnitude San Fernando earthquake in 1971 (Swanson & Sharma, 1979) is shown to be a result of its favourable orientation with respect to the rock mass geometry, evident by removability considerations alone.

Block theory fundamentals are presented by Goodman & Shi (1985), where proofs for all theorems can be found, and therefore will not be discussed here. A very helpful review of block theory is given by Goodman (1989) and recent developments in the application of block theory are summarized by Goodman (1995). Some essential concepts are briefly discussed below.

Manuscript received 12 January 1995; revised manuscript accepted 31 May 1996.
Discussion on this paper closes 1 December 1997; for further details see p. ii.
* Ben-Gurion University of the Negev, Beer Sheva.
† University of California, Berkeley.

Block theory assumptions

The application of block theory here assumes that discontinuity surfaces are perfectly planar, and extend entirely through the volume of interest; namely, discontinuities do not terminate within the region of a key block. New cracking is not considered and block deformation is neglected.

Mathematical concepts

The real power of block theory stems from its ability to distinguish between *removable* and *non-removable* half-space combinations. A block is the region of intersection of half-spaces formed by the discontinuities that form the block faces. A block is finite and removable if the conditions of Shi's theorem (Goodman & Shi, 1985) are met. In a rock mass with n non-parallel joint planes there are 2^n unique half-space intersections (joint pyramids, JPs), yet only a few are removable from a free face excavated through the system. Shi's theorem provides the solution for the removability of a block formed with a particular JP.

Mechanical concepts

We distinguish between two principal modes of failure:

(*a*) *lifting* or *falling*, when the block loses contact on all faces, and
(*b*) *sliding*, which can occur on any face individually or on two non-parallel faces simultaneously along their line of intersection. In the lifting mode, the direction of initial block motion coincides with the direction of the resultant force acting on the block. The sliding mode is divided into single and double face sliding. In single face sliding, the normal to the plane of sliding, the resultant force and the direction of sliding are all coplanar. In double face sliding, the direction of sliding is parallel to the line of intersection of the two boundary planes on which the block slides simultaneously.

Forces that are frequently considered in engineering are represented in block theory using vector analysis as well as stereographic projection. If the components of any force vector $\boldsymbol{F}$ are (X, Y, Z), then the magnitude of $\boldsymbol{F}$ is $|\boldsymbol{F}| = (X^2 + Y^2 + Z^2)^{1/2}$ and the direction cosines of $\boldsymbol{F}$ are

$$\hat{f} = \left(\frac{X}{|\boldsymbol{F}|}, \frac{Y}{|\boldsymbol{F}|}, \frac{Z}{|\boldsymbol{F}|}\right) \tag{1}$$

such that $\boldsymbol{F} = |\boldsymbol{F}|\hat{f}$.

A series of coincident forces $F_1, F_2, \ldots, F_n$ is usually replaced in block theory applications with its resultant $\boldsymbol{R}$:

$$\boldsymbol{R} = \sum_{i=1}^{n} \boldsymbol{F}_i = \left(\sum_{i=1}^{n} X_i, \sum_{i=1}^{n} Y_i, \sum_{i=1}^{n} Z_i\right) \tag{2}$$

Friction force is a reaction to sliding, and hence acts in the opposite direction to the direction of sliding. If $\boldsymbol{N}_i$, $i = 1, \ldots, n$ are the magnitudes of the normal reaction forces from each sliding plane, then the resultant friction force is

$$\boldsymbol{R}_\mathrm{f} = -\sum_{i=1}^{n} (N_i \tan \phi_i)\hat{s} \tag{3}$$

where ϕ_i is the friction angle on plane i and $\hat{s}$ is the sliding direction, assuming a Mohr–Coulomb criterion with zero cohesion for the shear strength of the sliding plane.

Water pressures acting on the faces of a block produce a water force ($\boldsymbol{R}_\mathrm{w}$) in the direction of the inward normal ($-\hat{n}_i$) of each face that experiences the corresponding water head (a block theory convention is that the positive direction of a joint normal points out of the block and into the rock):

$$\boldsymbol{R}_\mathrm{w} = \sum_{i=1}^{n} S_i(-\hat{n}_i) \tag{4}$$

where S_i is the integral of water pressure times area over the whole submerged portion of face i.

THREE-DIMENSIONAL LIMIT EQUILIBRIUM ANALYSIS

When the rock mass structure is clearly defined and the block geometry is known, a block-theory-based rock slope stability analysis can be performed using the following steps:

(*a*) block theory removability and mode analysis
(*b*) limit equilibrium analysis
(*c*) support dimensioning.

The stability analysis utilizes the 'friction circle' concept and the three-dimensional solution for the slip of a tetrahedral wedge using vector analysis (Wittke, 1965) or the stereographic projection (Londe *et al.*, 1969, 1970; John, 1968; Goodman, 1976). The basic components of this solution are shown in Fig. 1 using a lower hemisphere stereographic projection.

The advantage of the friction circle concept is that it defines the three-dimensional locus of 'safe' resultants acting on the block. The influence of any additional force can thus be examined by correctly rotating the resultant force, using stereographic projection procedures or vector operations. An example is shown in Figs 2 and 3, where a water force ($\boldsymbol{U}_k$) is acting on joint J_k. The original resultant ($\boldsymbol{W}$) is rotated to a new orientation ($\boldsymbol{R}_0$) along a great circle connecting $\boldsymbol{W}$ and $\boldsymbol{U}_k$ by the

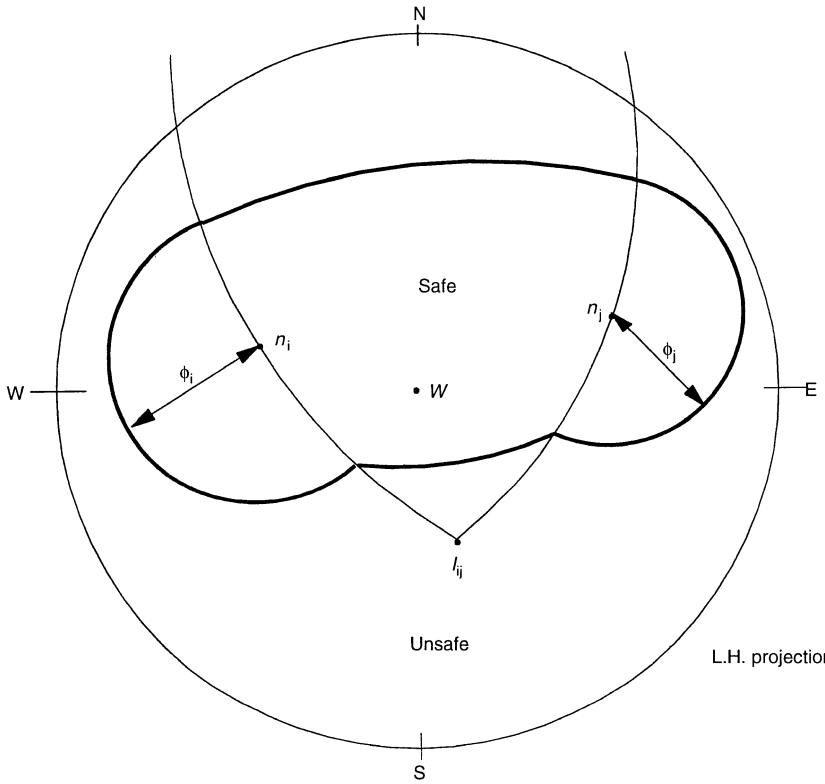

Fig. 1. Schematic presentation of the generalized friction circle for double face sliding (mode *ij*) of a tetrahedral block influenced by gravity loading (*W*) only (L.H., lower hemisphere)

angle α, the angle between the weight vector and the water force measured in their common plane (Fig. 3). It can be seen that the new orientation of the resultant force now plots inside the 'unsafe' locus, corresponding to sliding in the direction of the intersection $\boldsymbol{I}_{ij}$.

This procedure can be used to study the effect of water pressure inside a discontinuity (or tension crack) on the overall block stability. If it is found that the new resultant force is plotted within the unsafe zone for the analysed JP, no further analysis is required, as it can be stated that filling of a discontinuity with water is sufficient to drop the factor of safety against sliding below 1·0. If, however, the block remains safe, it is necessary to investigate the influence of water pressure that may develop inside the base joints.

To study the influence of water pressure inside the base joints, similar procedures are applied. Fig. 4 shows a two-dimensional pressure distribution that is assumed for the case where both of the base planes and the tension crack are filled with water (although the force on plane J_j is not shown). To find the new resultant force, the resultant water forces from all planes must be added: $\boldsymbol{R} = \boldsymbol{W} + \boldsymbol{U}_k + \boldsymbol{U}_i + \boldsymbol{U}_j$. In the absence of data regarding the exact position of the phreatic surface, it is impossible to know in advance the exact pressure distribution in each joint, and therefore the exact values of $\boldsymbol{U}_i$ and $\boldsymbol{U}_j$. In the analyses performed here a planar phreatic surface of uniform gradient above both joints is assumed, and the water heads above the centroid of each base plane, h_c, are assumed to be equal. This assumption permits a solution, calibrated for increasing heads, in both planes. A solution based on the above assumptions was proposed by Londe *et al.* (1970), who have used the fact that three vectors can be added in any desired order to reach the same final resultant:

$$\begin{aligned} &\boldsymbol{A} + \boldsymbol{B} = \boldsymbol{R}_{ab} \\ &\boldsymbol{A} + \boldsymbol{C} = \boldsymbol{R}_{ac} \\ &\boldsymbol{R}_{ab} + \boldsymbol{C} = \boldsymbol{R}_{ac} + \boldsymbol{B} = \boldsymbol{R}_{abc} \end{aligned} \tag{5}$$

This vector addition can be performed on the stereographic projection, using great circles to connect between two vectors that are added, and by measuring the angles between them in the correct direction. A construction corresponding to equation

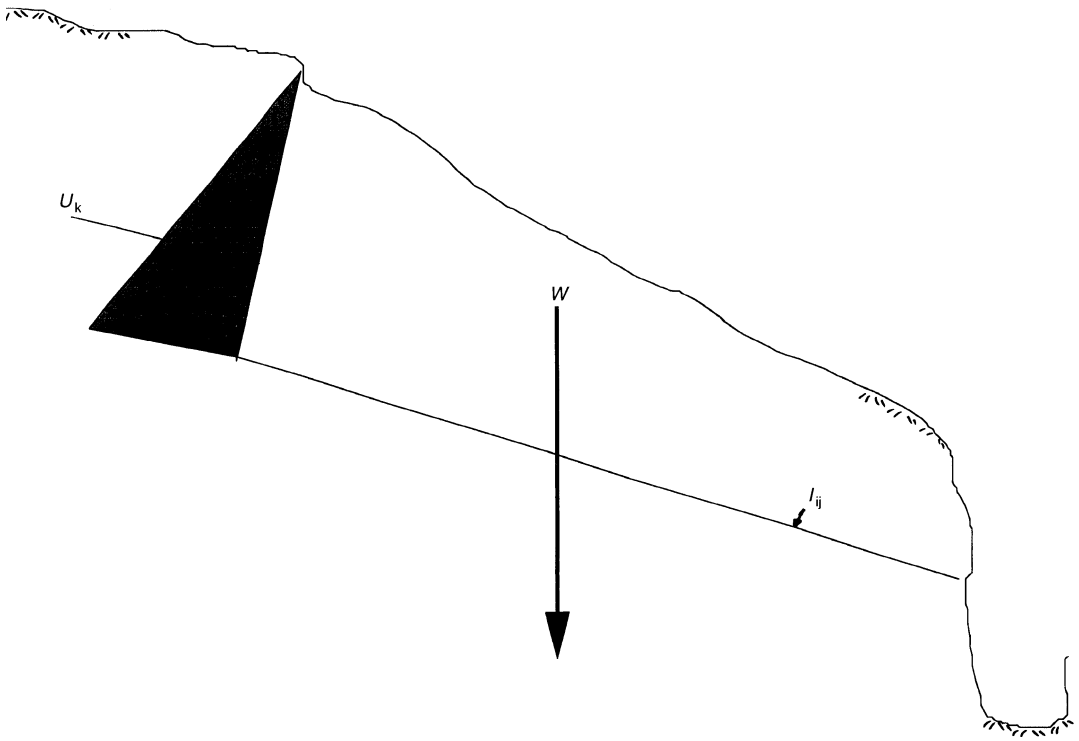

Fig. 2. Schematic cross-section parallel to I_{ij} showing a block with joint water force (U_k) inside a 'tension crack' (J_k)

(5) is shown in Fig. 5. This approach can be used to solve for resultants corresponding to increasing heads inside the base planes. The solution is based on the parametric addition of three vectors suggested by Londe *et al.* (1969, 1970) and discussed by Goodman (1976). Let $\boldsymbol{R}_0$ be the resultant of the block weight $\boldsymbol{W}$ and water force in the tension crack $\boldsymbol{U}_k$. Then we can say that

$$\boldsymbol{R}_0 + x\boldsymbol{U}_i + y\boldsymbol{U}_j = \boldsymbol{R}_0 + y\boldsymbol{U}_j + x\boldsymbol{U}_i = \boldsymbol{R} \qquad (6)$$

where x and y are variables corresponding to some head level in each joint. Using force polygons for $\boldsymbol{R}_0 + x\boldsymbol{U}_i$ and for $\boldsymbol{R}_0 + y\boldsymbol{U}_j$, the angle of rotation of $\boldsymbol{R}_0$ corresponding to each head level can be found. These angles can be scaled on the great circle connecting $\boldsymbol{R}_0$ and the corresponding water force, using the stereographic projections. A net of resultant paths emerges, and one can select the desired one to study the advance of the resultant at different loading conditions. A schematic illustration of the procedure is shown in Fig. 6, where the demonstrated resultant path (heavy line) corresponds to increasing head levels, of *equal* magnitudes, in both base planes simultaneously.

The factor of safety is defined as follows (Londe *et al.*, 1970):

$$FS = \frac{\tan \phi_{\text{available}}}{\tan \phi_{\text{required}}} \qquad (7)$$

A factor of safety of 1·0 represents limit equilibrium, where the resultant force plots on the boundary of the safe zone. Using the friction circle concept and the boundary between safe and unsafe zones, it is possible to read from the stereographic projection the *required* friction angle for stability under the given forces. This is the angle between the centre of the friction circle and the resultant, measured along a great circle that connects the two points. The *available* friction angle, a material property, is the angle between the centre of the friction circle and its circumference. It can be seen, therefore, that when the resultant plots outside the friction circle, the required friction angle is greater than the available friction angle. By equation (7), this leads to a factor of safety smaller than 1·0.

BACK-ANALYSIS OF TWO WEDGE FAILURES AT PACOIMA DAM

In this section an analysis of two catastrophic block failures which occurred at Pacoima Dam near Los Angeles, California, is described. The

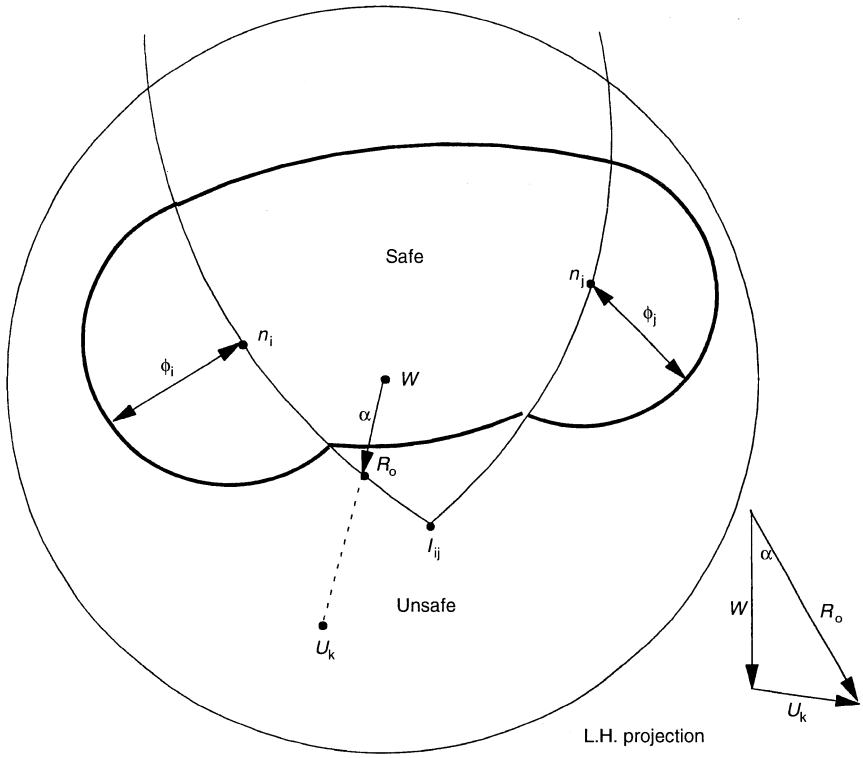

Fig. 3. Influence of the water force (U_k) on the orientation of the final resultant (R_0) and on the overall stability of the block

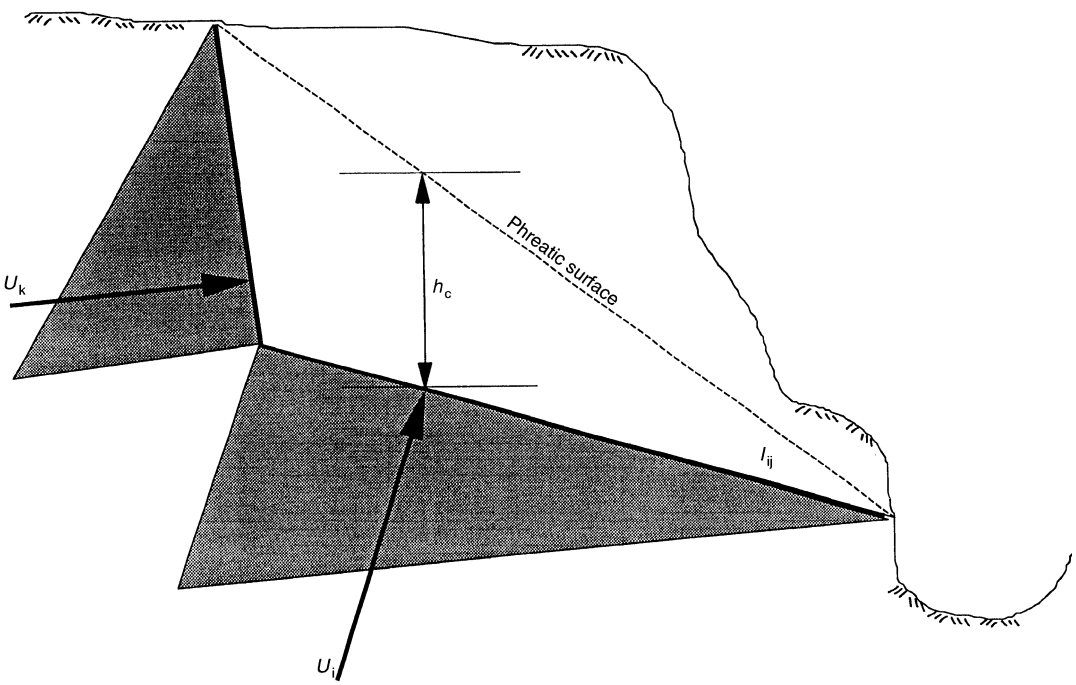

Fig. 4. Schematic cross-section parallel to I_{ij} showing assumed joint-water pressure distribution inside J_k and J_i

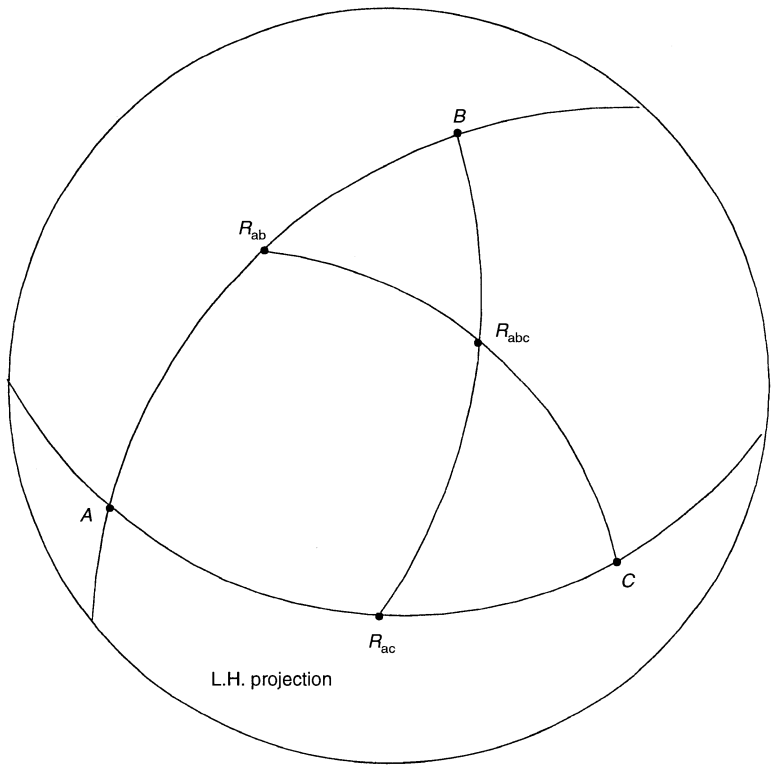

Fig. 5. Schematic diagram showing addition of three vectors by the intersection of three great circles, performed on the stereographic projection

input data are based on geological, structural and mechanical data collected in the field. The analysis is performed using the techniques discussed above. Some striking conclusions emerge, with respect to the influence of pressure head in joints, joint friction and block geometry on overall block stability.

Historical documentation of the failures

An eye-witness account of the case study is quoted below (Kuess, 1966).

> The spring of 1938 was noted by high intensity rainfall and a heavy runoff which produced spillway flow and large valve releases. These discharges eroded rock and created vibration in the area that resulted in two significant failures. Approximately 50 ft. downstream from the base of the dam, the first rock fall extends from stream bed upward some 200 ft. The breakaway occurred along one of the vertical ESE striking joints and was triggered by undercutting and vibration caused by valve release. The second failure occurred north and adjacent to the spillway. Thousands of yards of rock were released from the stream bed and up to near the crest of the ridge, to a point less than 100 ft. from the buttress. Water debouched from the spillway half way up the slope back in 1938, so that erosion and vibration were profound while spillway flow was in progress. The breakaway plane was apparently along one of the NW dipping joints with the crown controlled by the vertical shears.

General setting

Pacoima Dam is located in Pacoima Wash on the southern side of the San Gabriel Mountains, approximately 7 km north-east of San Fernando, California. The rocks of the area are derived from intrusion of dioritic magma into a sedimentary rock series. Schistose rocks in the area are the metamorphosed remnants of the sediments. The predominant rock type is quartz diorite gneiss, or diorite gneiss. Associated with the diorite gneiss are minor amounts of quartz monzonite, granite, gabbro, quartz veins, pegmatite and altered rock.

Rock structure

In order to characterize the principal joint sets, three scan-lines were performed in which a total of 173 joints were measured. The overall joint struc-

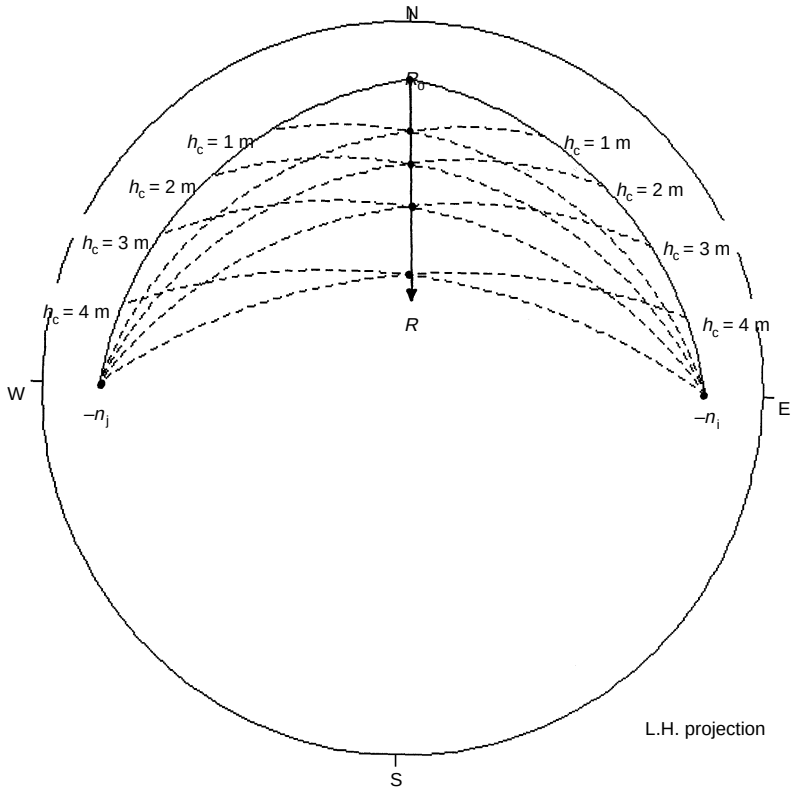

Fig. 6. Schematic diagram showing parametric addition of three vectors using the stereographic projection, assuming equal heads above the centroid of the base joints

ture is illustrated in the upper hemisphere projection of poles (Fig. 7), which shows the clustering of joint orientations. Four joint sets are recognized and their structural attributes are shown in Table 1, where the frequency is corrected for bias using Terzaghi's correction (Terzaghi, 1965).

Joint shear strength

Most joints in the field are tight and free of filling material, except for a few where a cohesionless filling material was sampled. The joint planes are therefore assumed to be non-cohesive. A friction angle of 30° was estimated for all joint sets, on the basis of tilt tests and characteristic roughness profiles. The sensitivity of the stability analysis to the value of the friction angle is studied in depth below.

Analysis of spillway failure

During the flood of 1938 the water that discharged from the spillway chute caused a large rock-slide in the valley in which the spillway is located. A photograph from 1940 shows the cavity of the block that was released during that event (Fig. 8(b) and (c)). The block was formed by a combination of a lower half-space of a member of the foliation set (J_1), an upper half-space of a member of the face maker joint (J_2) and an upper half-space of a member of the NW dipping joint set (J_3) (Fig. 9). The removability of the block is demonstrated by means of block theory removability analysis in Fig. 10, using an upper hemisphere stereographic projection, where the joints are shown in solid lines and the free face is dashed. The region corresponding to the block is shown (JP 100). A limit equilibrium analysis for this block is shown in Fig. 11, assuming a 30° friction angle on both joint surfaces. Note that a significant rotation of the resultant force ($\boldsymbol{W}$) is necessary for the block to become unstable and slide on the line of intersection of J_2 and J_3 ($\boldsymbol{I}_{23}$). When the active resultant force is parallel to gravity ($\boldsymbol{W}$ in Fig. 11), it plots within the safe zone. When the tension crack, in this case a member of the foliation planes (see Fig. 9) is filled with water, the new resultant force ($\boldsymbol{R}_0$) still plots within the safe zone. In Fig. 12, contour lines of equal friction are superimposed on the limit equilibrium plot. It can be seen

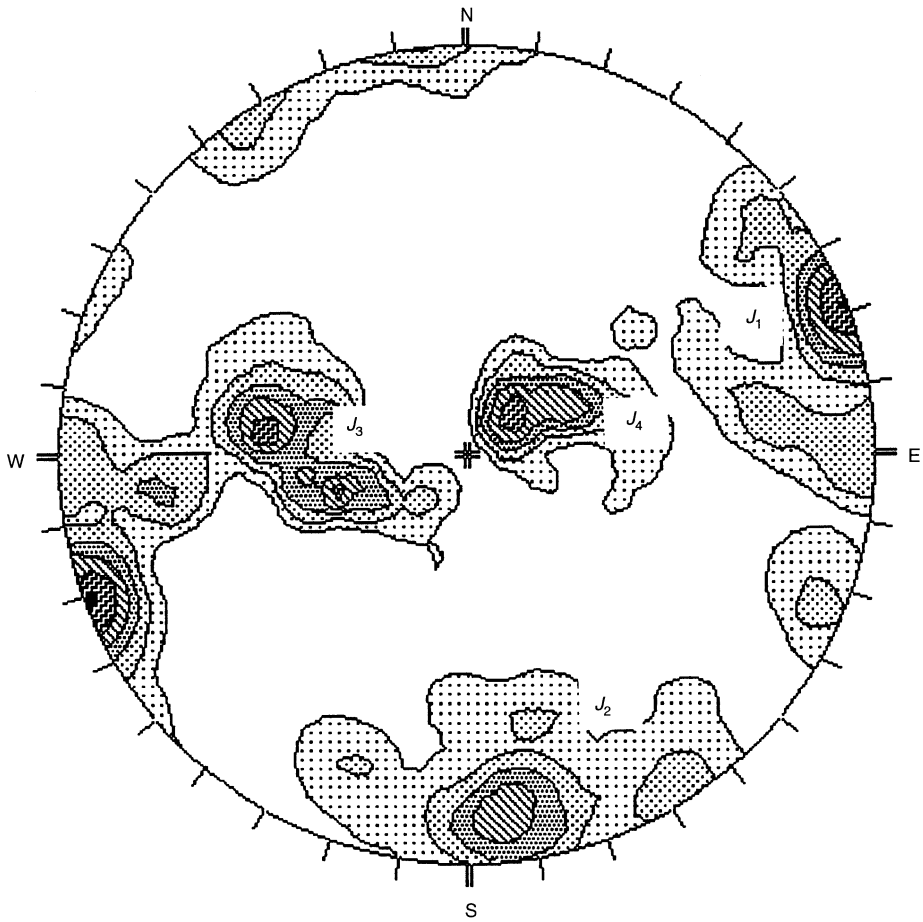

Fig. 7. Upper hemisphere projection of discontinuity pole distribution as measured at Pacoima Dam

Table 1. Principal joint set attributes

Joint set No.	Discontinuity type and name	Mean attitude (dip/dip direction)	Frequency: 1/m	Mean spacing: m
1	Foliation	84/78	0·22	4·6
2	Joints 'Face maker'	82/170	0·5	1·98
3	Shears	44/264	0·33	3
4	Faults 'Shallow dipping'	28/65	0·2	4·9

that the friction angle required to maintain stability of the block with the tension crack filled is 20°. Since the available friction angle is 30°, the factor of safety for this case is 1·59 (by equation (7)).

Because the block did slide, water pressures inside the base planes must be considered as well. An equal head for both base planes is assumed. Using the procedure discussed above, a solution is calibrated for increasing pressure heads from 0·1 m (0·98 kN/m^2) to 1 m (9·8 kPa) in 0·1 m increments. For each pressure level, the rotation of the resultant force is calculated using pressures from both planes, and the path that describes the rotation of the resultant force is obtained (Fig. 13). It can be seen that a pressure head of 0·25 m (2·45 kPa) is sufficient to rotate the resultant force from a safe position into the unsafe zone where sliding on the line of intersection takes place.

Note that with increasing head the resultant position dictates double face sliding in mode $\boldsymbol{I}_{23}$. If the

Fig. 8. (a) general view of Pacoima Dam; note the spillway at the left abutment releasing water after the 1938 flood; (b) side view of the spillway after the failure; (c) top view of the spillway block failure; photographs courtesy of Los Angeles County Department of Public Works

head level is raised above 0·6 m, however, the sliding mode is changed. The mode change is further studied in Fig. 12(a), an enlarged plot of the analysis shown in Fig. 11 with superimposed contours of equal friction angle values (2° intervals). Limit equilibrium is attained when the resultant plots on the contour of the *available* friction angle. Thus for each resultant position the friction angle contour on which it plots indicates the *required* friction angle for limit equilibrium. The required friction angle values for each head level increase are plotted in Fig. 12(b). It can be seen that a friction angle of 74° is required for a pressure head of 0·6 m to develop. If that pressure does develop, the resultant will dictate sliding in mode 3, that is, single face sliding on J_3. Furthermore, if theoretically the friction angle was as high as 90°, a pressure head of 1 m would have failed the block in *lifting*, namely the block would separate from all boundary planes and float, out of its position.

The influence of pressure head increase on the factor of safety, assuming a friction angle of 30°, is

Fig. 8. (*Continued*)

studied in Fig. 12(c). It can be seen that the rate of change of safety factor with respect to the pressure head in the base planes decreases when the failure mode changes from double face sliding to single face sliding. The results of this analysis therefore suggest that double face sliding is more easily triggered than single face sliding, for a given block geometry. This finding is supported by the results of another back-analysis—the study of the canyon wall failure in the left abutment.

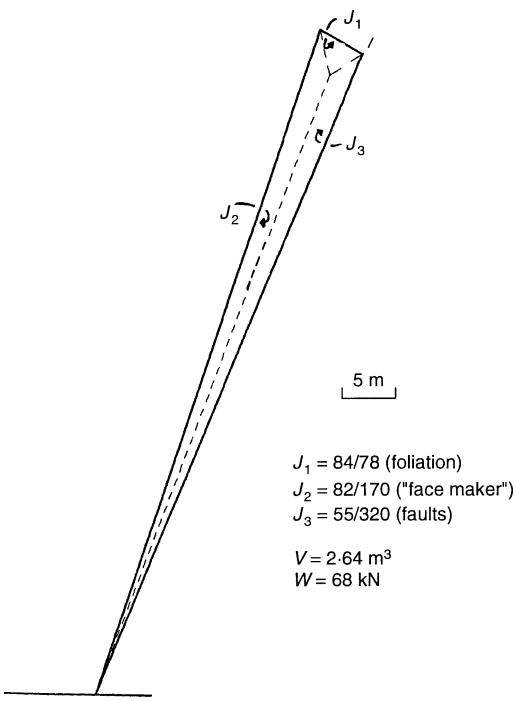

Fig. 9. Exact geometry of the spillway block

Analysis of left abutment failure

Another large block failure developed as a result of the 1938 flood in the canyon downstream from the dam. The block slid out of the left abutment rock, and the resulting debris pile can still be seen in the river bed today. The debris and the surface from which the block was separated are shown in Fig. 14. The block is formed by the intersection of the upper half-space of the foliation planes (J_1), the lower half-space of the face maker joint set (J_2) and the upper half-space of the shears (J_3) (Fig. 15). Since the joint surfaces are not accessible at present, the mean orientations of the joint sets were used for analysis. The removability of the block from the slope of the canyon is demonstrated in Fig. 16 (JP 010). As in the case of the spillway block, we first evaluate the stability of the block under gravitational force alone (Fig. 17). It can be seen that the block is stable under its own weight ($\boldsymbol{W}$) and under the new resultant ($\boldsymbol{R}_0$) with water pressure in a filled tension crack (J_2). Using a contour plot of lines of equal friction superimposed on the diagram in Fig. 17, it can be seen that $\boldsymbol{R}_0$ plots on the contour of $\phi = 10°$ (Fig. 18(a)). With an available friction angle of 30°, the factor of safety for that condition is 3·27.

To find the level of water pressure that must have developed inside the base joints to initiate sliding, equal heads inside both base planes (J_1 and J_3) were assumed. The pressure head was then increased from 2 m (19·6 kPa) to 20 m (196 kPa)

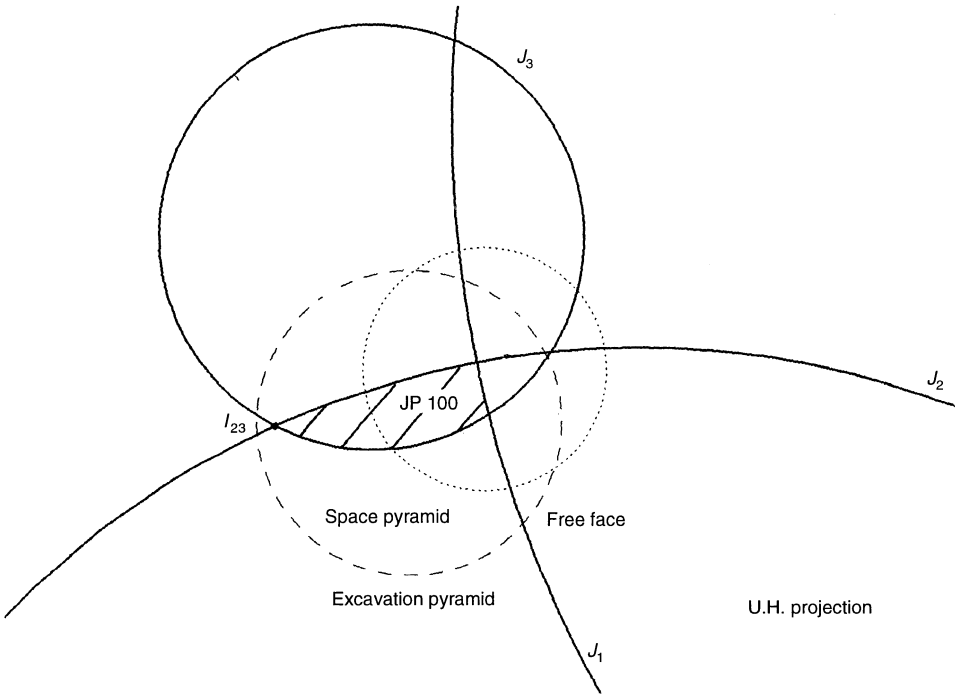

Fig. 10. Block theory removability analysis of the spillway block (JP 100) (U.H., upper hemisphere)

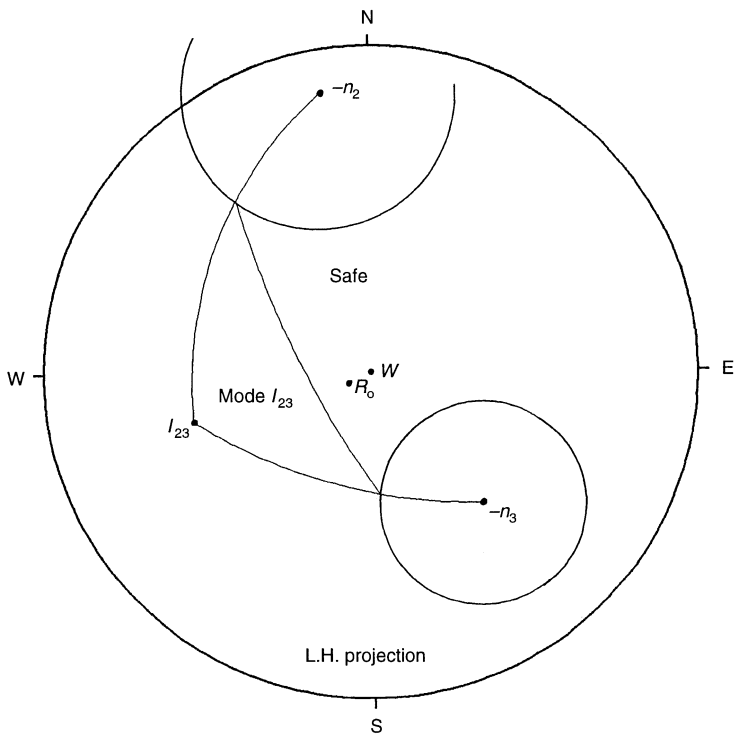

Fig. 11. Limit equilibrium analysis of the spillway block for a water-filled 'tension crack' (J_1)

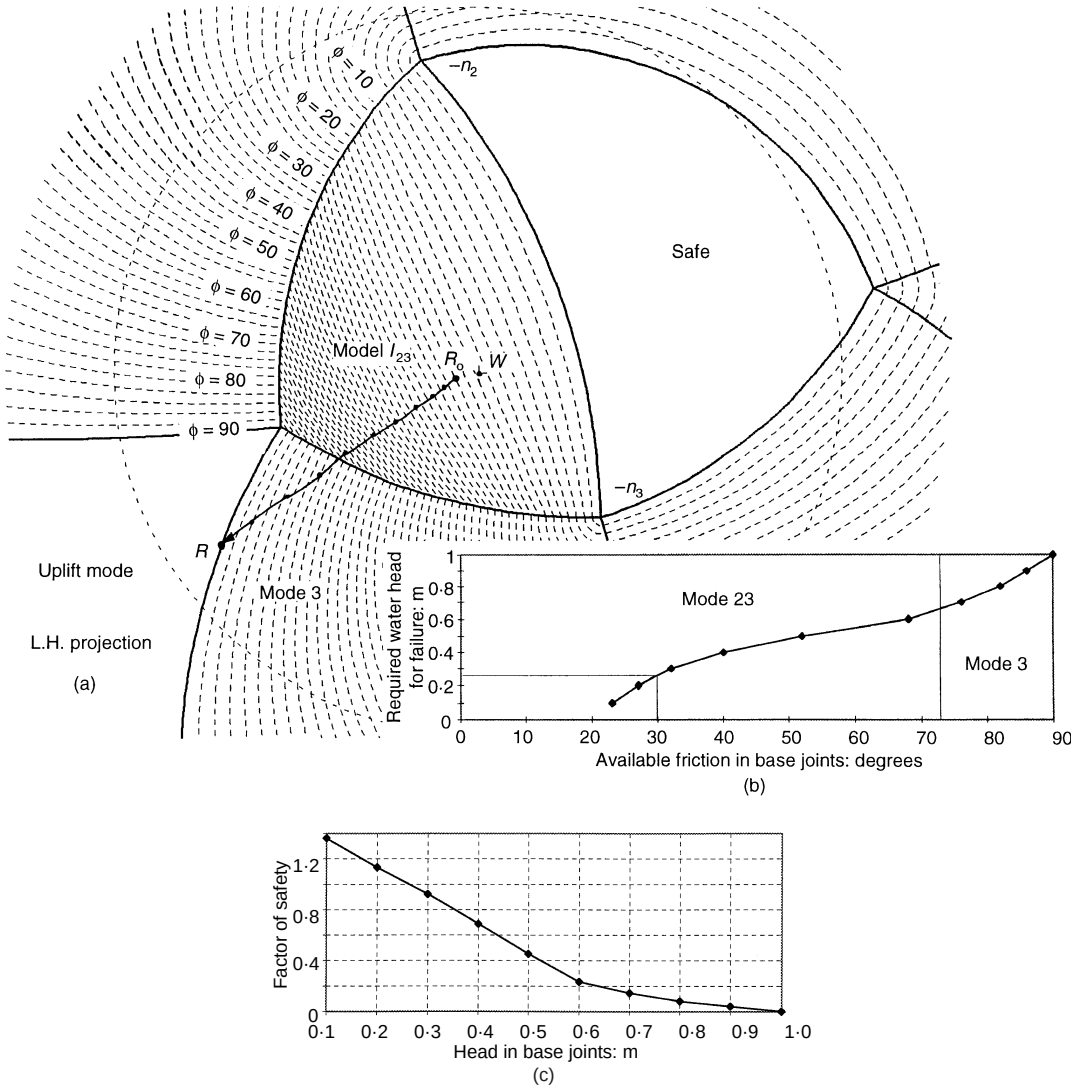

Fig. 12. (a), (b) sensitivity analysis showing influence of available friction angle on the critical water head at which sliding ensues; contours represent iso-friction values in 2° intervals; location of resultant force vector (*R*) under increasing water heads is shown by points representing head increase steps of 0·1 m; (c) sensitivity analysis showing influence of head increase on factor of safety

in steps of 2 m, and the rotation of the resultant force in each interval was calculated and plotted (Fig. 19). When the pressure head reached 8 m (78 kPa) the resultant force (***R***) rotated into the unsafe region.

The analysis shown in Fig. 18 allows inspection of the change in failure mode as loading of the block progresses. The region of failure mode $\boldsymbol{I}_{13}$ is defined by the locus bounded by the great circles connecting $-\boldsymbol{n}_1$, $-\boldsymbol{n}_3$ and $-\boldsymbol{I}_{13}$ and the locus of mode 3 is the spherical triangle connecting $-\boldsymbol{I}_{13}$, $\boldsymbol{I}_{23}$ and $\boldsymbol{n}_3$ ($\boldsymbol{I}_{23}$ is not shown). The particular geometry of the block dictates the path of the resultant force under the applied pressures. It can be seen that owing to the given geometry the resultant travels within the safe zone up to a pressure head of 8 m. When that pressure is exceeded, the resultant force emerges in the mode 3 zone, similar in essence to the behaviour of the spillway block. In this case, however, the analysis is not merely academic but of practical significance because the required friction angle for a mode change is only 30°, beyond which failure commences by sliding on plane 3 (Fig. 18(b)).

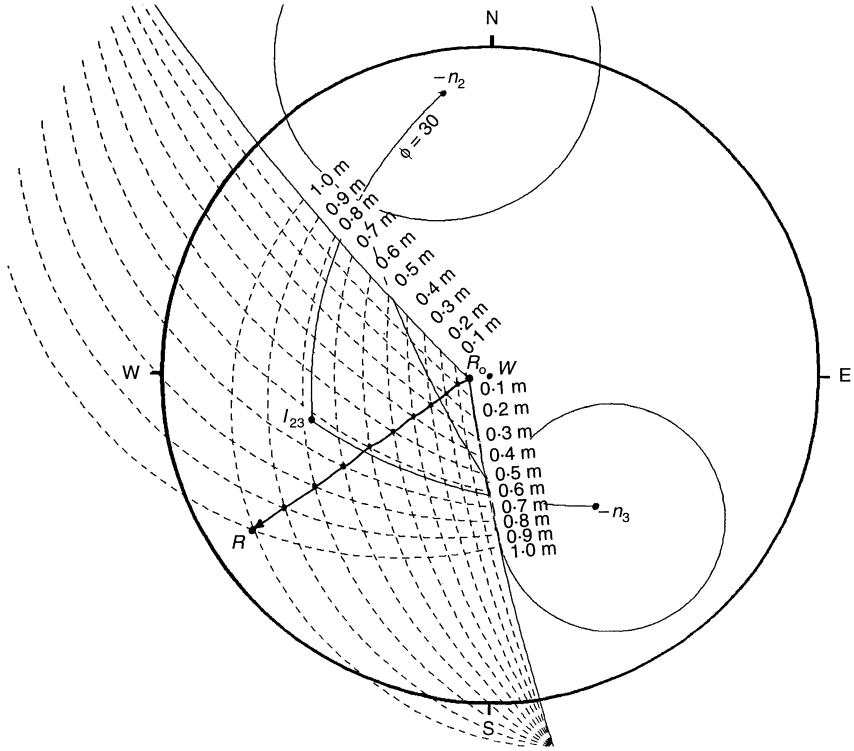

Fig. 13. Travel path of the resultant force acting on the spillway block starting from a filled tension crack (R_0) through pressure steps of 0·981 kPa in both side planes (equivalent to 0·1 m water head above centroids in both base planes)

Investigation of the sensitivity of the factor of safety to the critical pressure head (Fig. 18(c)) validates the result suggested by the analysis of the spillway failure. It is again shown that the rate of change of the factor of safety decreases when the sliding mode changes from double face to single face sliding.

The mechanical response of the blocks to pressure head loading explored in this section is entirely dictated by the geometry of the boundary planes, because water pressures are, by nature, always normal to the discontinuity surface, and are directed into the block interior. Only a fully three-dimensional analysis could reveal this complex failure mechanism. Another three-dimensional aspect of block stability, its removability, is explored in the following section.

BLOCK THEORY STABILITY ANALYSIS OF RIGHT ABUTMENT

Historical background

Throughout the service life of Pacoima Dam, from its completion in 1929 to the present, there have been few stability problems associated with the right abutment. Two significant historical events attest to that, the 1938 flood discussed above and the 1971 San Fernando earthquake. During the massive flood of 1938, all the damage was concentrated at the left abutment. Two large rock-slides, triggered by the flood, were analysed above. The right abutment, however, remained intact. Furthermore, the source of the 1971 San Fernando earthquake, which registered 6·6 on the Richter scale, was located almost directly below Pacoima Dam (Gere & Shah, 1984). Extremely large ground accelerations, over 1·0g, were recorded at the top of the dam, and the canyon below was subjected to numerous small landslides. There were indications that the base-rock acceleration might have been in the range of 0·6 to 0·8g (Swanson & Sharma, 1979). Following the earthquake, significant ground displacements of two large rock masses were measured in the left abutment. The right abutment, however, performed very well during that event, and ground displacements were not noticed (Swanson & Sharma, 1979).

The significance of free face orientation

The relationship between rock geometry and free face orientation may be considered as the

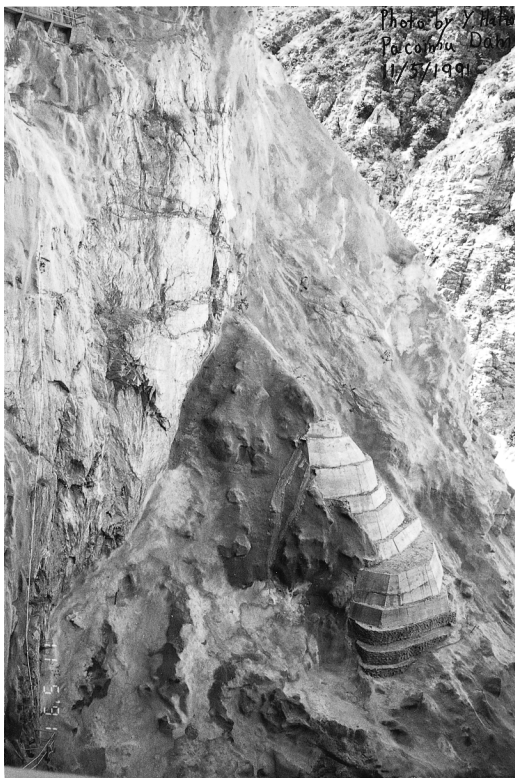

Fig. 14. Site of left abutment failure

single, most significant factor affecting rock slope stability in competent–discontinuous rock masses. In cases where a joint plane or a line of intersection of two joint planes dips into the free face and 'daylight', plane failures or wedge failures respectively may be expected. This has been demonstrated using the two cases analysed above, where slippage occurred. A three-dimensional analysis, in this case block theory analysis, allows detection of such failure mechanisms and timely installation of appropriate support. The same analysis method may also prove that a given slope is perfectly safe, owing to the removability consideration. The study of Pacoima Dam provides an example of such a case where favourable orientation of the rock mass with respect to the right abutment put that abutment in a safe category, unlike the opposite left abutment, as will be shown below.

Analysis

The right abutment stability can be explained by means of the critical-key-block method of analysis developed by Hatzor (1992) and discussed by Hatzor & Goodman (1992, 1993). In this method we look at all possible joint combinations (JCs) and find the removable JP of each, with respect to the analysed free face. In the case of Pacoima Dam there are four joint sets and therefore four joint combinations must be analysed, assuming the most likely blocks are tetrahedral (Hatzor, 1992).

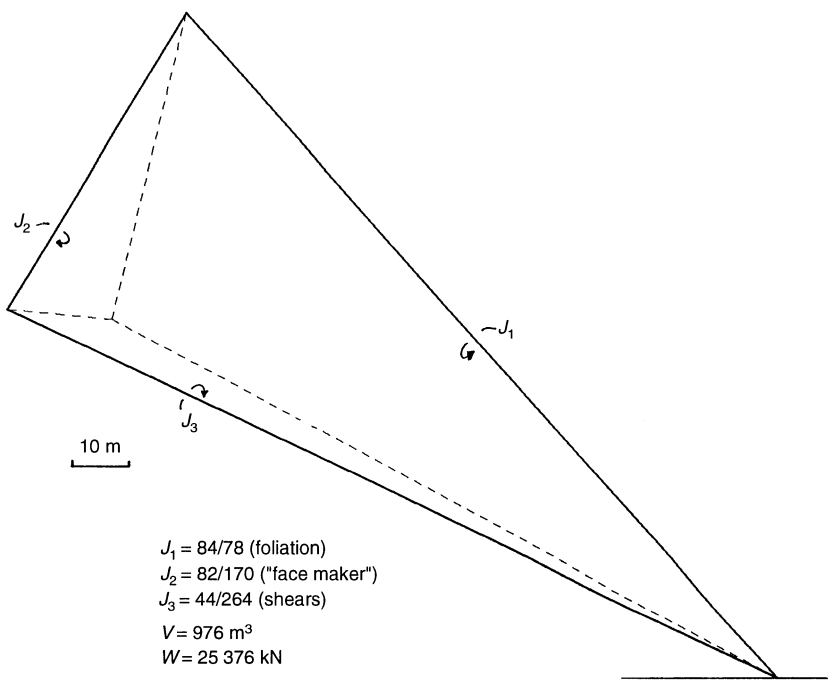

Fig. 15. Exact geometry of the left abutment block

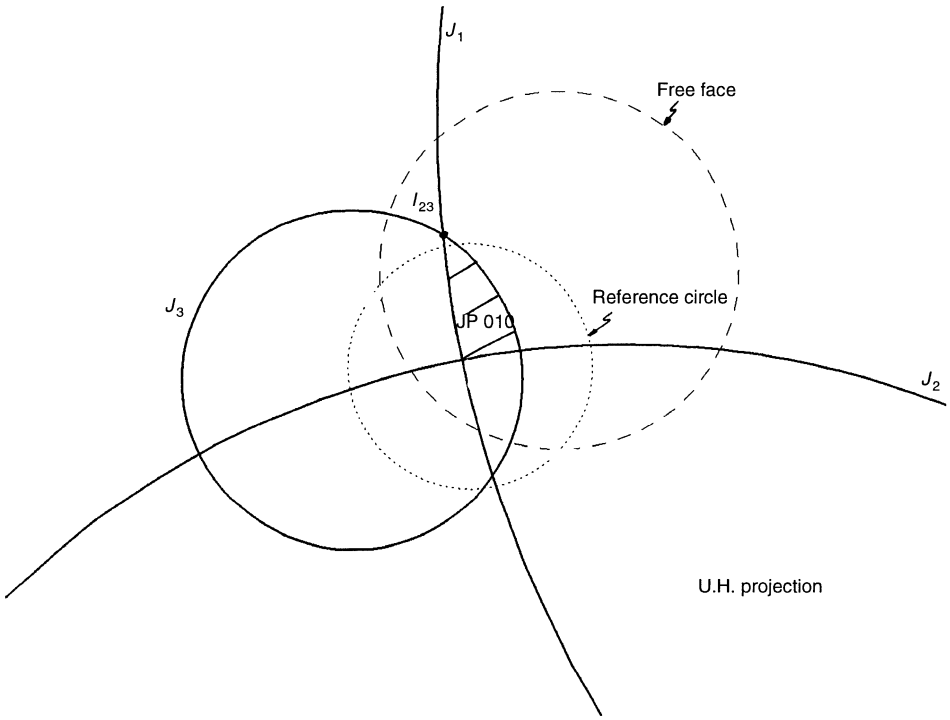

Fig. 16. Block theory removability analysis for the left abutment block (JP 010)

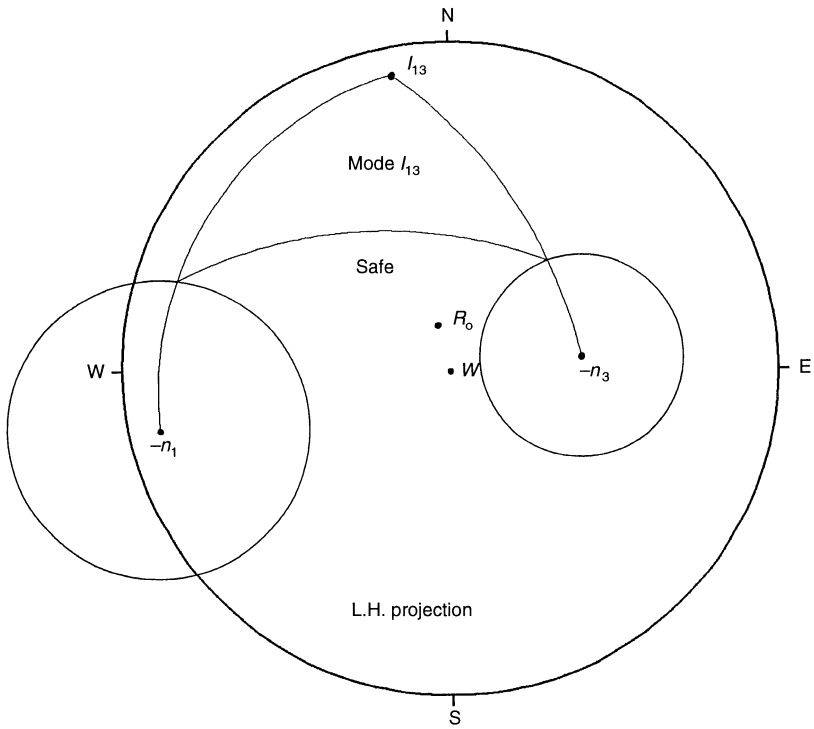

Fig. 17. Limit equilibrium analysis for the left abutment block

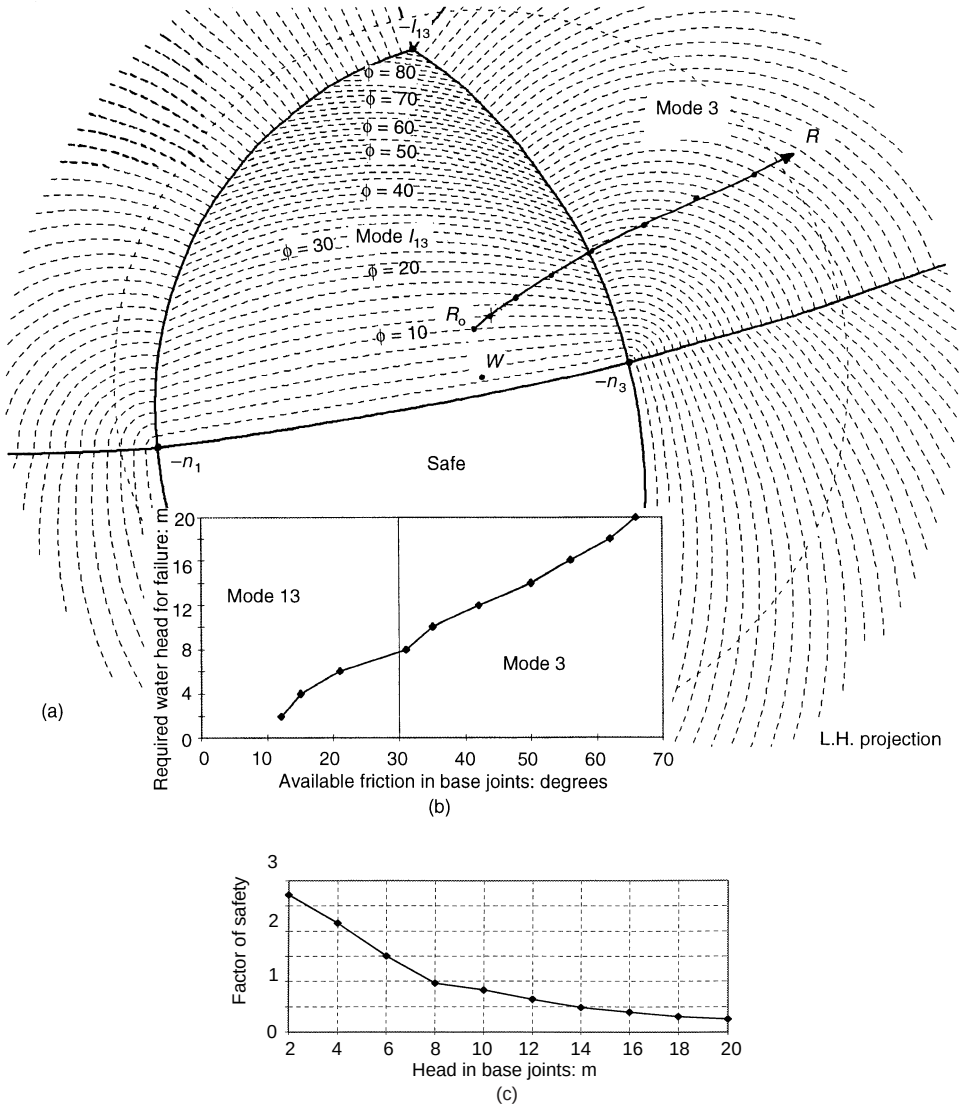

Fig. 18. (a), (b) sensitivity showing influence of available friction angle on the critical water head at which sliding ensues (water head is increased by 2·0 m steps starting from 2 m up to 20 m; (c) sensitivity analysis showing influence of increasing head on factor of safety

The results of removability analysis are shown in Table 2 and in Fig. 20.

Every joint combination forms one JP which is removable from the right abutment free surface. The critical-key-block method of analysis assigns a relative block failure likelihood value for each removable JP. The block failure likelihood $P(B)$ is a product of three independent parameters: joint combination probability (P(JC)), joint pyramid shape parameter (K) and the JP instability parameter (F). The mathematical derivation of the three parameters is developed by Hatzor (1992) and reviewed by Hatzor & Goodman (1993). The predictive capability of $P(B)$ is demonstrated, using two tunnelling case studies, by Hatzor & Goodman (1992), and the goodness of fit for each individual parameter (P(JC), K and F) is studied by Hatzor (1993).

The results of the critical-key-block analysis performed for all removable JPs are shown in Table 3 and in Fig. 21. Fig. 21 clearly shows that there are only two JPs of concern: JP 100 of JC(1) and JP 001 of JC(4). Fig. 20 shows the removability analysis for each joint combination for the

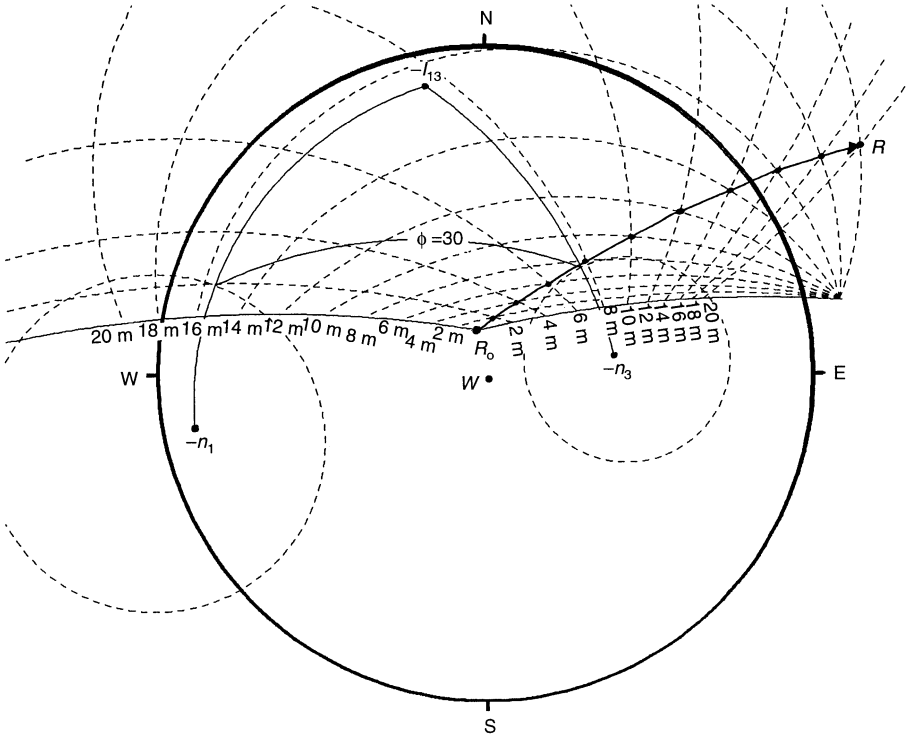

Fig. 19. Travel path of the resultant force vector starting from a filled tension crack (R_0) through pressure steps of 19·62 kPa (equivalent to 2 m water head above the centroid of each base joint)

Table 2. Joint combinations and removable blocks for right abutment

JC (No.)	J_i; J_j; J_k	JP ⊂ SP Results of removability analysis
1	123	100; 000 Edge; no mode
2	124	100 No mode
3	134	001 No mode
4	234	001; 000 Edge; no mode

right abutment free face (dashed). JC(1) is analysed in Fig. 20(a), where two JPs plot inside the space pyramid: JP 100 and JP 000 (unlabelled). JP 000 has no mode and therefore is not removable even if the friction angle on the joints is zero degrees. JP 100 is not removable because it has one edge ($\boldsymbol{I}_{23}$) which plots on the contour of the free surface. This is a rare case producing *non-harzardous* blocks, as discussed by Hatzor & Goodman (1993). This same line of intersection appears in JC(4) and therefore a similar result is obtained there (Fig. 20(d), Table 2). JC(2) and JC(3) both produce removable blocks which have no mode: JP 100 in JC(2) and JP 001 in JC(3) (Figs 20(b) and (c), Table 2). Thus it can be seen that owing to the particular interaction between free face orientation and rock mass geometry in the right abutment, that abutment is safe against block sliding. This result is obtained as a consequence of the occurrence of non-hazardous blocks which have a common edge with the free face.

Figure 22(a) shows a synthetic generation of joint traces on the right abutment created by JC(1)—the JC with the highest relative intersection probability. The trace map generation procedure used here follows the techniques of Shi *et al.* (1985) and Shi & Goodman (1989). Fig. 22(b) shows the traces of JP 100 of JC(1) after all the trees and branches are cut off so that only removable areas remain (Shi & Goodman, 1989). It can be seen that even if the realization of the joints in the right abutment deviates slightly from the ideal orientations so that *removable* rather than non-hazardous JPs form (where all lines of intersections plot within the space pyramid), the removable area would only be a small proportion (7·75%) of the

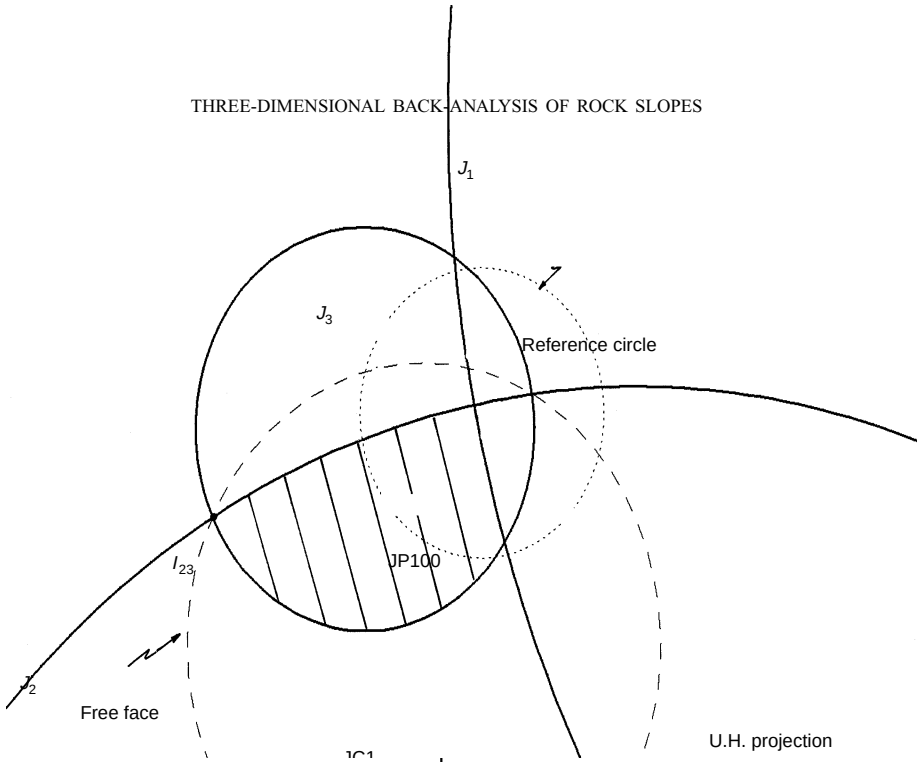

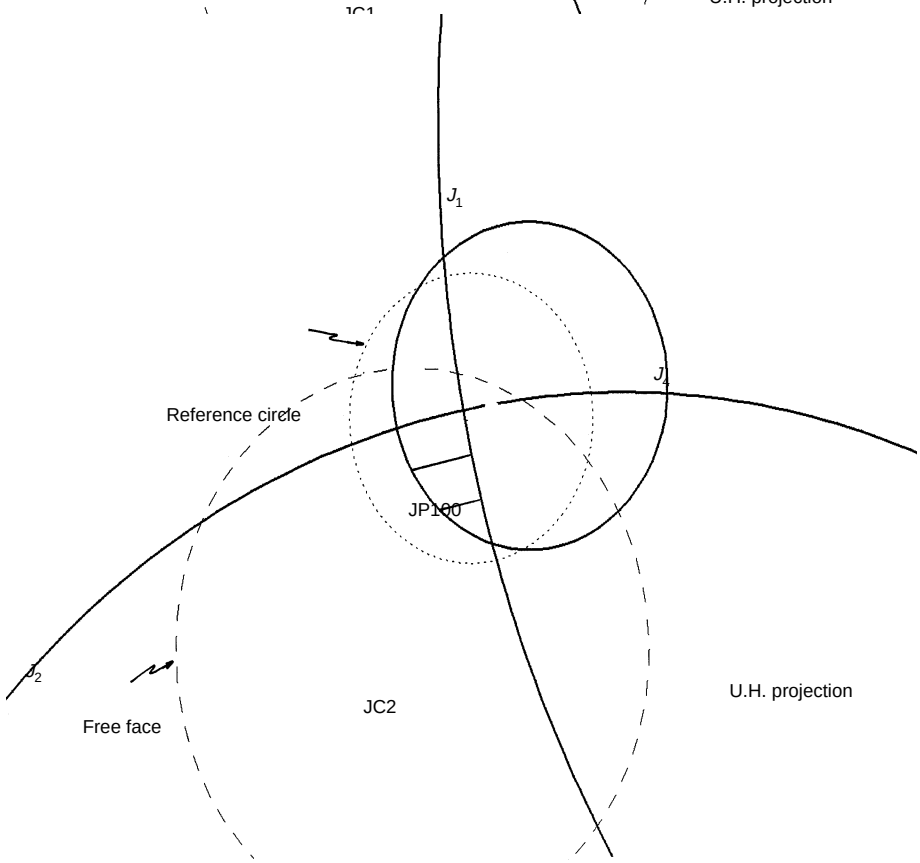

(b)

Fig. 20. Block theory removability analysis for the four possible joint combinations in the right abutment of Pacoima Dam: (a) JC1; (b) JC2; (c) JC3; (d) JC4

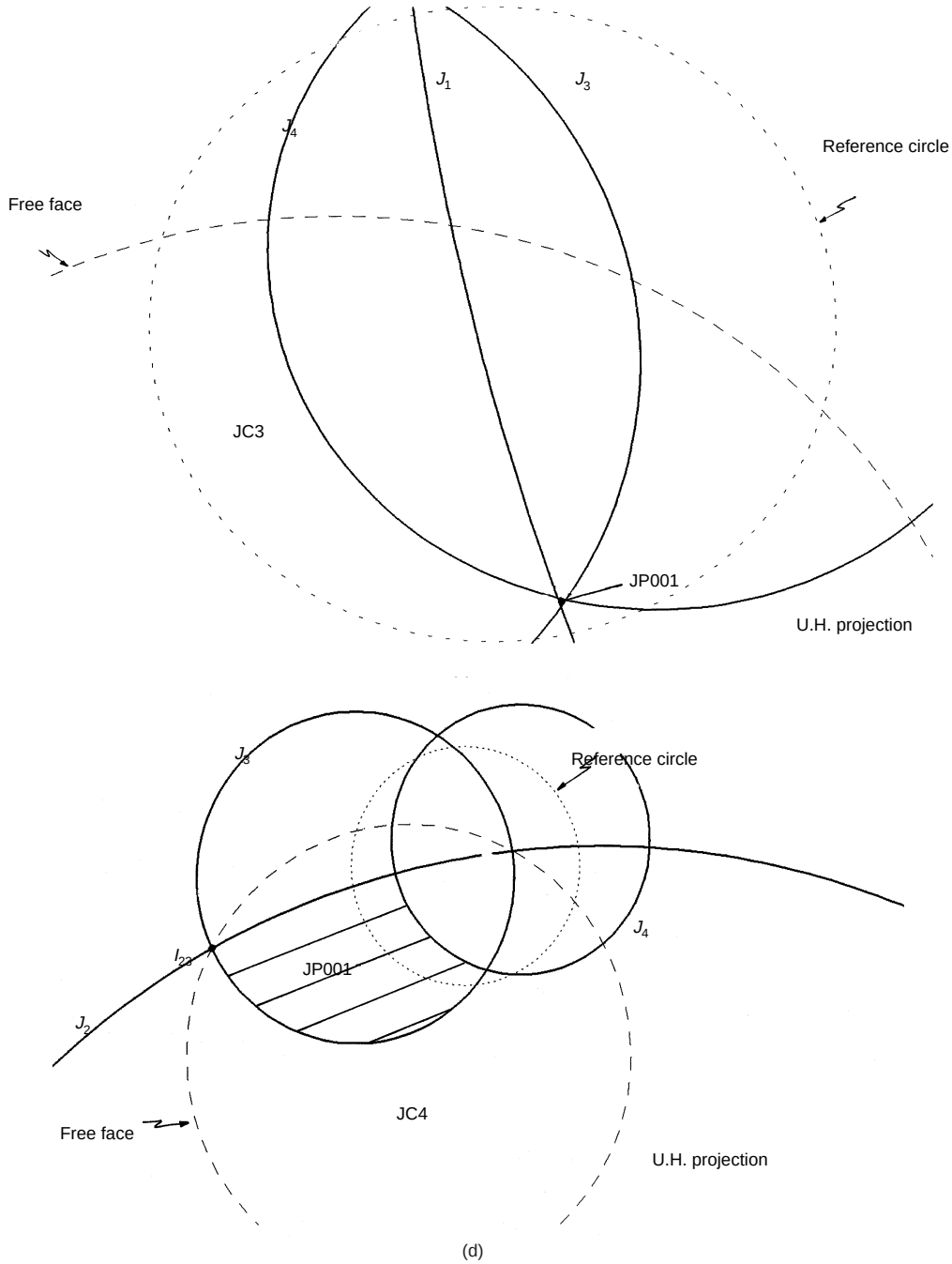

Fig. 20. (*Continued*)

total abutment area. Thus, should removable blocks materialize in some locations at the right abutment by joint combination 1, their influence on overall stability would be negligible. Goodman (1995), in his comprehensive review of block theory, also discussed the results concerning the relatively low risk associated with the right abutment, using Fig. 22. He has shown that this conclusion led to the

Table 3. Results of critical key block analysis (free face orientation 59/197)

JC No.	J_{ijk}	JP code	P(JC)	K	F	$P(B)$
1	J1, J2, J3	100	$7{\cdot}11 \times 10^{-4}$	0·171	1·165	$1{\cdot}42 \times 10^{-4}$
2	J1, J2, J4	100	$4{\cdot}52 \times 10^{-4}$	0·077	No mode	0
3	J1, J3, J4	001	$8{\cdot}24 \times 10^{-6}$	$3{\cdot}3 \times 10^{-5}$	No mode	0
4	J2, J3, J4	001	$8{\cdot}49 \times 10^{-6}$	0·094	1·165	$9{\cdot}31 \times 10^{-5}$

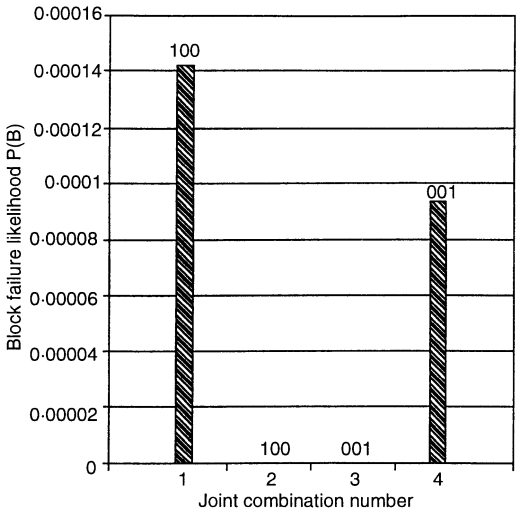

Fig. 21. Block failure likelihood values for all joint combinations

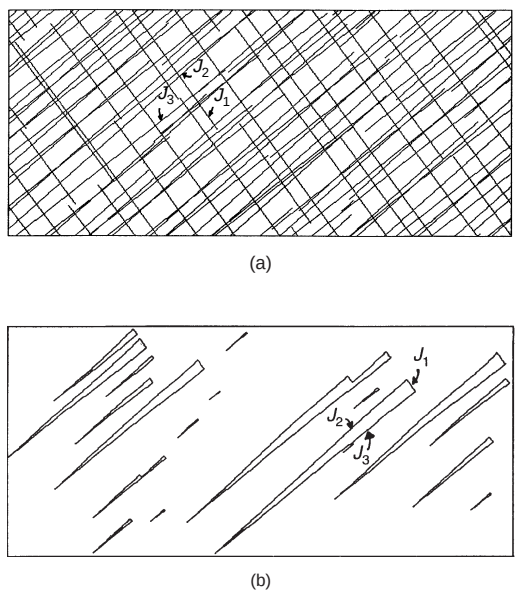

Fig. 22. Statistical joint trace generation of joint combination 1 as it would appear on the right abutment of Pacoima Dam (presently concealed by gunite): (a) joint trace map for JC(1); (b) trace map of the critical key block area on the right abutment

decision to construct a new supplementary chute spillway on the right abutment, with the discharge conducted to avoid spillage against the sensitive left abutment.

The conclusion obtained here by means of block theory removability analysis is strongly supported by field evidence: the good performance the right abutment exhibited along its history of turmoil, while visited by a severe flood and several events of strong ground accelerations.

SUMMARY AND CONCLUSIONS

The application of analytical tools, particularly limit equilibrium, mode and block removability analysis, has been demonstrated, in the context of block failures at Pacoima Dam.

The application of block-theory-based analysis with water pressures has been demonstrated using two rock failures that occurred following a flood in 1938. Several lessons can be learned from the back-calculation of these failures:

(*a*) The orientation of the active resultant changes rapidly with increasing pressure heads that develop inside the block boundary planes. Plotting the active resultant at each increase of pressure revealed that pressure can change the failure mode. In the two cases analysed here the failure mode changed from double face to single face sliding as the water pressure increased.

(*b*) The actual realization of mode change depends on the available friction angle which provides the resistance to block sliding during pressure head build-up. In one case (the so-called spillway failure) it was shown that the mode change, from double to single face sliding, required a friction angle of 74°, and a pressure head of only 0·6 m above the centroid of the base joints (after the tension crack at the back of the block had been completely filled). In another case (the left abutment failure), the

same failure mode change occurs at a pressure head of 8 m but requires a friction angle of only 30°, the value assumed in the analysis here.

(*c*) The influence of pressure head build-up on the factor of safety was investigated as well. It was shown graphically (Figs 12(c), 18(c)) how the factor of safety decreases with increasing pressure head. It was found that the rate of change of the factor of safety with respect to pressure head decreases when the mode changes from double face to single face sliding. Therefore, for a given block geometry, a given increase of pressure head will reduce the factor of safety in the case of double face sliding more rapidly than in the case of single face sliding.

(*d*) The single most important factor influencing rock slope stability in competent—discontinuous rock masses is the interaction between the rock mass geometry and the orientation of the free surface. When this relationship is unfavourable, rock failures should be expected, as was shown using the spillway and left abutment failures of Pacoima Dam. When this relationship is favourable, the rock slope may be assumed safe, as proved by the integrity of the right abutment of Pacoima Dam. Using block theory these conditions can be tested quite readily.

(*e*) The development of water pressures along block boundaries (discontinuity apertures) should be avoided as much as possible. It has been shown that relatively small water pressures acting over a large area of discontinuity surface mobilized sizeable blocks, which were otherwise safe against sliding.

ACKNOWLEDGEMENTS

We would like to acknowledge the support of Wolfgang H. Roth of Dames and Moore, Los Angeles, and the assistance provided to us in the field by Michael Johnson of Los Angeles County Department of Public Works.

REFERENCES

Bray, J. W. (1966). Limiting equilibrium of fractured and jointed rock. *Proc. 1st Congress ISRM, Lisbon*, Vol. 1, pp. 531–535.

Bray, J. W. (1967). A study of jointed and fractured rock. Part II: Theory of limiting equilibrium. *Felsmechanik* **4**, 197–216.

Bray, J. W. & Brown, E. T. (1976). A short solution for the stability of a rock slope containing a tetrahedral wedge. *Int. J. Rock Mech. Min. Sci. & Geomech. Abstr.* **13**, 227–229.

Gere, J. M. & Shah, H. C. (1984). *Terra non firma*. Stanford, CA: Stanford Alumni Association.

Goodman, R. E. (1976). *Methods of geological engineering in discontinuous rocks*. St Paul, West Publishing Co.

Goodman, R. E. (1989). *Introduction to rock mechanics*, 2nd edn. New York: Wiley.

Goodman, R. E. (1995). Block theory and its applications. 1995 Rankine Lecture. *Géotechnique* **45**, No. 3, 383–423.

Goodman, R. E. & Shi, G.-H. (1985). *Block theory and its application to rock engineering*. Englewood Cliffs: Prentice-Hall.

Goodman, R. E., Karaca, M. & Hatzor, Y. (1993). *Rock structure in relation to concrete dams on granite*, pp. 56–68. Geotechnical Special Publication No. 35, ASCE.

Hatzor, Y. (1992). Validation of block theory using field case histories. PhD thesis, Department of Civil Engineering, University of California, Berkeley.

Hatzor, Y. (1993). The block failure likelihood: a contribution to rock engineering in blocky rock masses. *Int. J. Rock Mech. Min. Sci. & Geomech. Abstr.* **30**, No. 7, 1591–1597.

Hatzor, Y. & Goodman, R. E. (1992). Application of block theory and the critical key block concept to tunneling: two case histories. *Proc. Conf. on Fractured and Jointed Rock Masses* (eds L. R. Myer, N. G. W. Cook, R. E. Goodman & C. Tsang), pp. 663–670. Rotterdam: Balkema.

Hatzor, Y. & Goodman, R. E. (1993). Determination of the design block for tunnel supports in highly jointed rock. In *Comprehensive rock engineering*. Vol. 2. *Analysis and design methods* (ed. C. Fairhurst), pp. 263–292. Oxford: Pergamon Press.

Hoek, E. & Bray, J. W. (1981). *Rock slope engineering*. London: Institution of Mining and Metallurgy.

Jaeger, J. C. (1971). Friction of rocks and stability of rock slopes. *Géotechnique* **21**, No. 2, 97–134.

John, K. W. (1968). Graphical stability analysis of slopes in jointed rock. *J. Soil Mech. Fdns Div., ASCE* **94**, No. SM2, 497–526.

Kuess, H. A. (1966). *Resumé of the geology, groundwater, and rock treatment with specific reference to the left (South) abutment*. Unpublished report, submitted to Los Angeles County Department of Public Works.

Londe, P. F., Vigier, G. & Vormeringer, R. (1969). Stability of rock slopes, a three dimensional study. *J. Soil Mech. Fdns Div., ASCE* **95**, No. SM7, 235–262.

Londe, P. F., Vigier, G. & Vormeringer, R. (1970). Stability of rock slopes—graphical methods. *J. Soil Mech. Fdns Div., ASCE* **96**, No. SM4, 1411–1434.

Shi, G.-H., Goodman, R. E. & Tinucci, J. P. (1985). Application of block theory to simulate joint trace maps. *Proc. Int. Symp. on Fundamentals of Rock Joints, Bjorkliden*, pp. 367–383. Rotterdam: Balkema.

Shi, G.-H. & Goodman, R. E. (1989). The key blocks of unrolled joint traces in developed maps of tunnel walls. *Int J. Numer. Anal. Methods Geomech.* **13**, 131–158.

Swanson, A. A. & Sharma, R. P. (1979). Effects of the 1971 San Fernando earthquake on Pacoima arch dam. *Commission Internationale Des Grands Barrages,*

New Delhi, pp. 797–824.
Terzaghi, K. (1962). Stability of steep slopes on hard unweathered rock. *Géotechnique* **12**, No. 4, 251–270.
Terzaghi, R. D. (1965). Sources of error in joint surveys. *Géotechnique* **15**, 287–304.
Wittke, W. (1965). Methods to analyse the stability of rock slopes with and without additional loading. *Rock Mech. Engng Geol.*, Supp. II. (In German).